



# Ultrastructural observations of mitochondrial morphology through the life cycle of the brown alga, *Mutimo cylindricus* (Cutleriaceae, Tilopteridales)

Yuan Shen<sup>1,2</sup> · Taizo Motomura<sup>2</sup> · Chikako Nagasato<sup>2</sup>

Received: 18 April 2021 / Accepted: 1 June 2021 / Published online: 17 June 2021  
© The Author(s), under exclusive licence to Springer-Verlag GmbH Austria, part of Springer Nature 2021

## Abstract

Mitochondrial morphology varies according to development and the physiological conditions of the cell. Here, we performed electron tomography using serial sections to analyze the number, individual volume, and morphological complexity of mitochondria in the cells across two generations in the life cycle of the brown alga *Mutimo cylindricus*. This species shows a heteromorphic alternation of generations between the macroscopic gametophyte and the crustose sporophyte during its life cycle and displays anisogamous sexual reproduction. We observed the mitochondria in the vegetative cells of gametophytes and sporophytes to mainly show tubular or discoidal shapes with high morphological complexity. The morphology of the mitochondria in the male and female gametes changed to a nearly spherical or oval shape from a tubular or discoidal shape before release. In this species, degradation of the paternal mitochondria was observed in the zygote 2 h after fertilization. Morphological changes in the mitochondria were not observed until 6 h after fertilization. Twenty-four-hour-old zygotes before and after cytokinesis showed a similar number of mitochondria as 6-h-old zygotes; however, the volume and morphological complexity increased. The results indicated that the maternal mitochondria did not undergo fission or fusion until this stage. Based on the analysis results of the number and total volume of mitochondria before and after the release of the gametes, it is possible that the mitochondria in the female gametes fuse immediately before release.

**Keywords** Brown algae · Electron microscopy · Life cycle · Mitochondria · Serial section tomography

## Introduction

Mitochondria are membrane-bound organelles with their own DNA and supply adenosine triphosphate (ATP), which is used as a source of chemical energy in cell activity. It is believed that morphological characteristics of the mitochondria, such as shape, size, and number, change throughout the life of a cell. This suggests that, morphologically, mitochondria vary depending on development, growth, differentiation, apoptosis, maturation, and aging (Chan 2012).

In unicellular organisms, following changes in mitochondrial morphology throughout the life cycle is comparatively easier, and in some cases, the life cycle may directly indicate the cell cycle. *Cyanidioschyzon merolae* possesses a single mitochondrion whose division, along with chloroplast division, precedes nuclear division. The mitochondria change their morphology into spherical, ovoid, and dumbbell-shaped structures before division and return to a spherical shape after division (Kuroiwa 2010; Yoshida et al. 2017). In the unicellular green alga *Chlamydomonas reinhardtii*, mitochondria form a tubular network toward asexual reproduction, and mitochondria in the liberated daughter cells exhibit a giant form and, subsequently, a thick- and thin-corded form (Ehara et al. 1995). However, during meiosis after conjugation, the mitochondrial morphology exhibits a continuous change into spherical, tubule-, branch-, and mesh-like structures (Aoyama et al. 2009).

In multicellular organisms, almost all studies relating to mitochondrial morphology have focused on a specific developmental period, such as gametogenesis, fertilization, or early

---

Handling Editor: Handling Editor: Tsuneyoshi Kuroiwa

✉ Chikako Nagasato  
nagasato@fsc.hokudai.ac.jp

<sup>1</sup> Graduate School of Environmental Science, Hokkaido University, Sapporo 060-0810, Japan

<sup>2</sup> Muroan Marine Station, Field Science Center for Northern Biosphere, Hokkaido University, Muroan 051-0013, Japan

embryonic development. Mitochondria in animal sperm exhibit characteristic features and maternal inheritance (Sato and Sato 2013). Morphological changes and the transition of mtDNA content during spermatogenesis can serve as a key to understanding the mechanism of maternal inheritance of this organelle. In mammals, to prevent the transmission of paternal mtDNA to the progeny, the number of nucleoid mitochondria gradually decreases during sperm formation (Rantanen and Larsson 2000). In addition, a drastic morphological transformation of the mitochondria is observed during spermatogenesis. The mitochondria in spermatogonia, leptotene, and zygotene spermatocytes are generally small and spherical. They elongate in pachytene spermatocytes and early spermatids, and fragment again in late spermatids (De Martino et al. 1979). In maturing spermatids, small mitochondrial spheres are regularly arranged across the midpiece, and they elongate as they wrap around the midpiece (Ho and Wey 2007). In the early stage of spermatogenesis in rabbits, mitochondrial cristae have been observed to become highly dilated during the transition phase between spermatogonia and primary spermatocytes (Nicander and Ploen 1969).

In a previous study, we clarified paternal inheritance of mitochondria in the anisogamous brown alga *Mutimo cylindricus* (Shen et al. 2020). We concluded that maternal inheritance of mitochondria could be universal in brown algae. In the case of *M. cylindricus*, observations of ultrathin sections indicated that the size of the mitochondria in the male and female gametes was almost identical. However, the average DNA content of one mitochondrion in male gametes was one-seventh of that in female gametes. Mitophagic digestion of paternal mitochondria occurs in zygotes. One of the mechanisms in uniparental inheritance of mitochondria in this species is the reduction of mitochondrial DNA in male gametes. However, the mechanism underlying the formation of robust mitochondria in female gametes is unclear.

All species of brown algae show multicellularity. Some of them alternate between the generation of diploid sporophytes and haploid gametophytes. *M. cylindricus* is an anisogamous species with a heteromorphic life cycle alternating between macroscopic gametophytes and microscopic sporophytes (Kitayama et al. 1992; Kawai et al. 2012). In this study, we examined mitochondrial morphology in gametophytes, gametangia, gametes, zygotes, and sporophytes through 3D analysis using transmission electron microscopy (TEM) on serial section images. In brown algae, 3D analysis has been performed using electron tomography (Terauchi et al. 2012; Fu et al. 2013; Nagasato et al. 2014; Kinoshita et al. 2016). Those studies revealed the structure of the plasmodesmata, transient membrane configuration during cytokinesis, and flagella. The present study is the first to demonstrate the 3D reconstruction of a structure using serial sections, focusing on the structure of brown algal mitochondria. These data enabled quantification of mitochondria in each target stage.

## Material and methods

### Culture

Mature male and female gametophytes of *M. cylindricus* (Okamura) H. Kawai and T. Kitayama (Kawai et al. 2012) were collected at Odanohama, Toba, Mie, Japan (34°45' N 136°87' E), in March 2015 and April 2019. Male and female individuals were identified based on the morphology of the plurilocular gametangia under a light microscope. Unialgal cultures of *M. cylindricus* were established from gametes or trichothallic hairs of male and female gametophytes (Shen et al. 2020) and incubated in sterilized seawater containing half-strength Provasoil's enriched seawater medium (Provasoli 1968). Gametogenesis and maturation were induced under the following conditions: 15 °C, using white-light-emitting diodes (LEDs, 20–40  $\mu\text{mol photons m}^{-2} \text{s}^{-1}$ ) and long-day conditions (14-h light:10-h dark). The release of gametes was stimulated by exchanging the fresh culture medium the day before and by light the next day. Male and female gametes were collected separately in microtubes on ice. Fertilization was induced by adding male gametes to settled female gametes on a gel support film (ATTO, Tokyo, Japan) in Petri dishes.

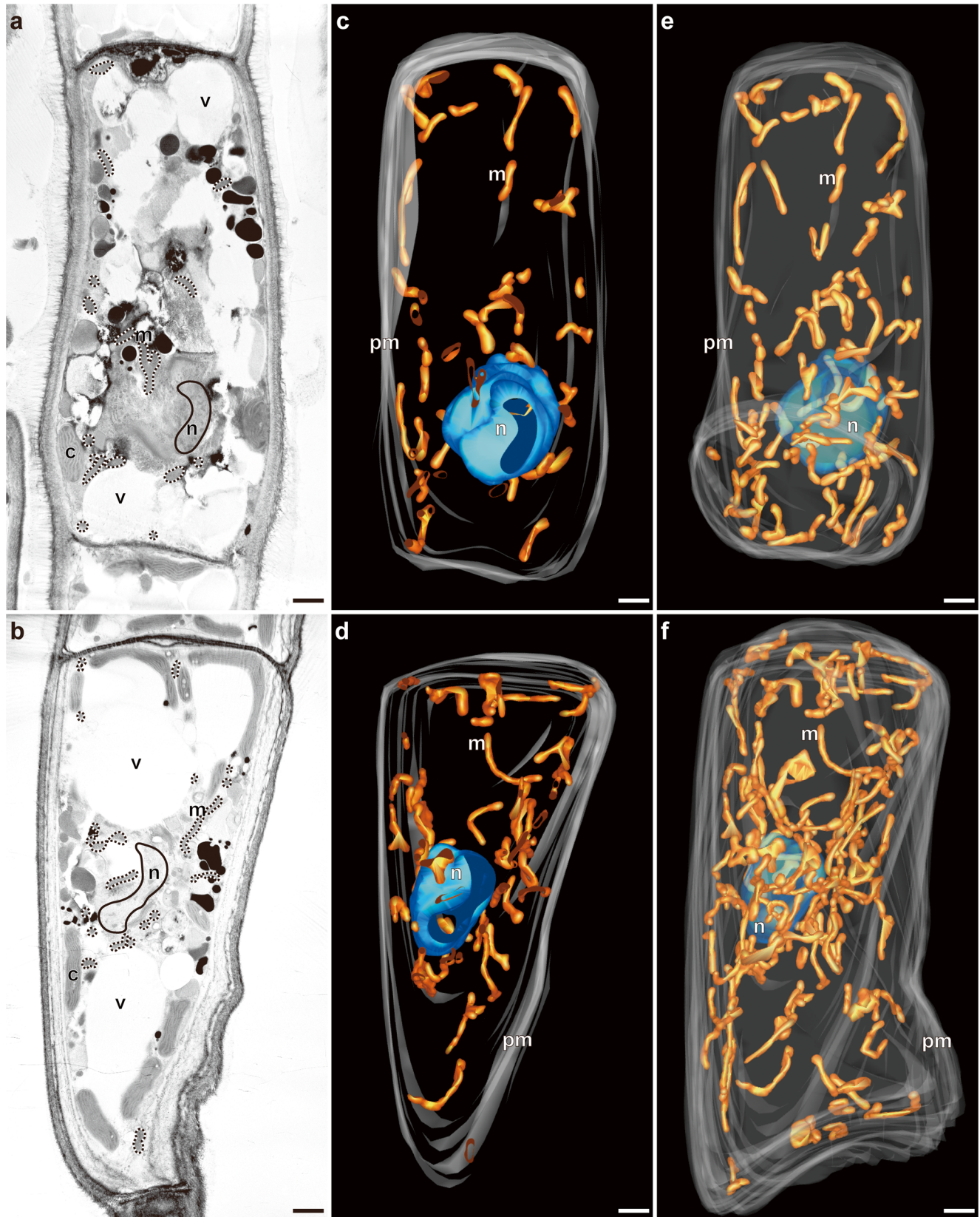
### Cryofixation and freeze-substitution for TEM samples

Rapid freezing and freeze substitution by the immersion method were applied to the male and female gametes, 2-, 6-, and 24-h-old zygotes, and two-, four-, and seven-celled sporophytes on the gel support film. The gametes were collected as pellets following centrifugation at 500 $\times$ g for 1 min using a KUBOTA model 4000 centrifuge (KUBOTA, Tokyo, Japan). The pellets were then placed and spread on a formvar-coated gold ring immediately before freezing. The gel support films containing the just fertilized and developing specimens were cut into triangular shapes < 1 cm<sup>2</sup> (Nagasato and Motomura 2002). The gametes on the gold rings, or early zygotes on the gel support films, were rapidly immersed in a pre-cooled liquid propane bath (−186 °C) and subsequently transferred into liquid nitrogen. Gametophytes and 20-day-old crustose sporophytes were frozen using high-pressure

**Fig. 1** Mitochondrial morphology in the somatic cells of gametophytes. **a, c, e** Male gametophyte, **b, d, f** female gametophyte. **a** A thin-section image of male gametophyte. **b** A thin-section image of female gametophyte. **c** A partial 3D model of the nucleus, mitochondria, and plasma membrane reconstructed from serial thin sections in the same cell as **a**. **d** A partial 3D model of the nucleus, mitochondria, and plasma membrane reconstructed from serial thin sections in the same cell as **b**. **e** A complete 3D model of **c**. **f** A complete 3D model of **d**. c, chloroplast; pm, plasma membrane; m, mitochondrion; n, nucleus; v, vacuole. Scale bar: 1  $\mu\text{m}$

freezing. Thalli fragments were cut, placed into gold carriers, frozen using a high-pressure freezer (Leica Microsystems,

Vienna, Austria) at  $-196\text{ }^{\circ}\text{C}$  and 2100 bar, and then stored in liquid nitrogen.



Freeze-substitution was performed by transferring the frozen samples from liquid nitrogen to a freeze-substitution medium (2% osmium tetroxide [OsO<sub>4</sub>] dissolved in anhydrous acetone) pre-cooled in a liquid nitrogen cooling bath, and the samples were stored at −85 °C for 2 days. The samples were gradually warmed to −20 °C for 2 h, to 4 °C for 2 h, and then to room temperature for approximately 30 min. Next, the samples were washed several times with anhydrous acetone at room temperature and infiltrated with increasing concentrations (10%, 30%, 50%, 70%, 80%, 90%, and 100%) of low-viscosity Spurr's epoxy resin (Polysciences, Warrington, PA, USA). Finally, the samples were embedded in Spurr's epoxy resin in aluminum foil dishes.

Serial sections were cut using a NACC diamond knife (Micro Star Technologies, Huntsville, TX, USA) with an ULTRACUT ultramicrotome (Reichert-Jung, Vienna, Austria), mounted on formvar-coated slot grids, and stained using an EM stainer (Nisshin EM, Tokyo, Japan). The sections were observed using a JEM-1011 electron microscope (JEOL, Tokyo, Japan). Consecutive serial sections of each sample were examined. Images were acquired using TEM films (Fujifilm, Tokyo, Japan). The developed films were scanned and converted into digital data using an EPSON GT-X980 photo scanner (EPSON, Nagano, Japan) and images were standardized (tiff format, resolution 300 dpi, 8-bit grayscale).

### Three-dimensional reconstruction

Alignment of whole cell serial section images was performed using Fiji software (<http://fiji.sc/Fiji>, Lowe 2004; Schindelin et al. 2012; Murtin et al. 2018). The alignment method for the serial sections was modified from that described in previous studies. Stacks were made using two adjacent (source and target) images, and feature extraction was automatically performed using the scale-invariant feature transform (SIFT) algorithm. The images were aligned using the “Linear Stack Alignment with SIFT” plugin. The stack was converted into images, the transformed target image was treated as a new source image, and the next section was aligned as the target image.

For the 3D reconstruction of whole-cell serial section images, the sequence of transformed images was converted into stacks using the IMOD software package (version 4.9.12) (Kremer et al. 1996). The pixel sizes of several standardized section images were obtained using the “set scale” Fiji plugin according to the scale bar in each image (Supplementary Table S1). The thickness range of the sections was estimated based on the interference color of the ultrathin sections (Peachey 1958). Therefore, it was impossible to set the z-axis value, the ratio of section thickness (nm) to pixel size (nm), in the stacking of serial section images as accurately as in electron tomography. For this reason, the thickness was

calibrated using spherical organelles, such as small vacuoles (Cui et al. 2019). Finally, the mean thickness (approximately 100 nm) of each gold serial section was determined (Supplementary Fig. S1a, b). The 3D models were generated from the outlines of each object in the serial sections along the z-axis. The volumes and surface areas of individual intracellular structures (nuclei, mitochondria, plasma membrane) were obtained from the IMOD software and calculated using the program IMODINFO.

The mitochondrial complexity index (MCI) is a score between the mitochondrial surface area (SA) and volume (V) and is associated with mitochondrial shape complexity (Vincent et al. 2019). Based on 3D modeling of mitochondria, we calculated the index according to a previously reported formula:  $MCI = SA^3/16\pi^2V^2$  (Vincent et al. 2019). MCI is 0.71 for a spherically shaped mitochondrion and > 0.71 for an ellipsoid or tubular shape. A higher value indicates greater elongation or branching of the mitochondrion.

### Statistical analysis

All data shown are derived from three cells, with the exception of two- (24-h-old zygotes) or four-celled structures (four daughter cells from two 24-h-old zygotes after cytokinesis), from independent biological samples in each life-cycle stage (Supplementary Table S1; the corresponding 3D images are shown in Supplementary Fig. S2). All results are presented as mean ± standard error of the mean (SEM). Significant differences among different stages of the life cycle were determined using Tukey's multiple comparison test (Supplementary Table S2). Statistical tests were performed using GraphPad Prism software (version 8.0.2, GraphPad Software, Inc., San Diego, CA, USA).

## Results

### Biological material used in this study

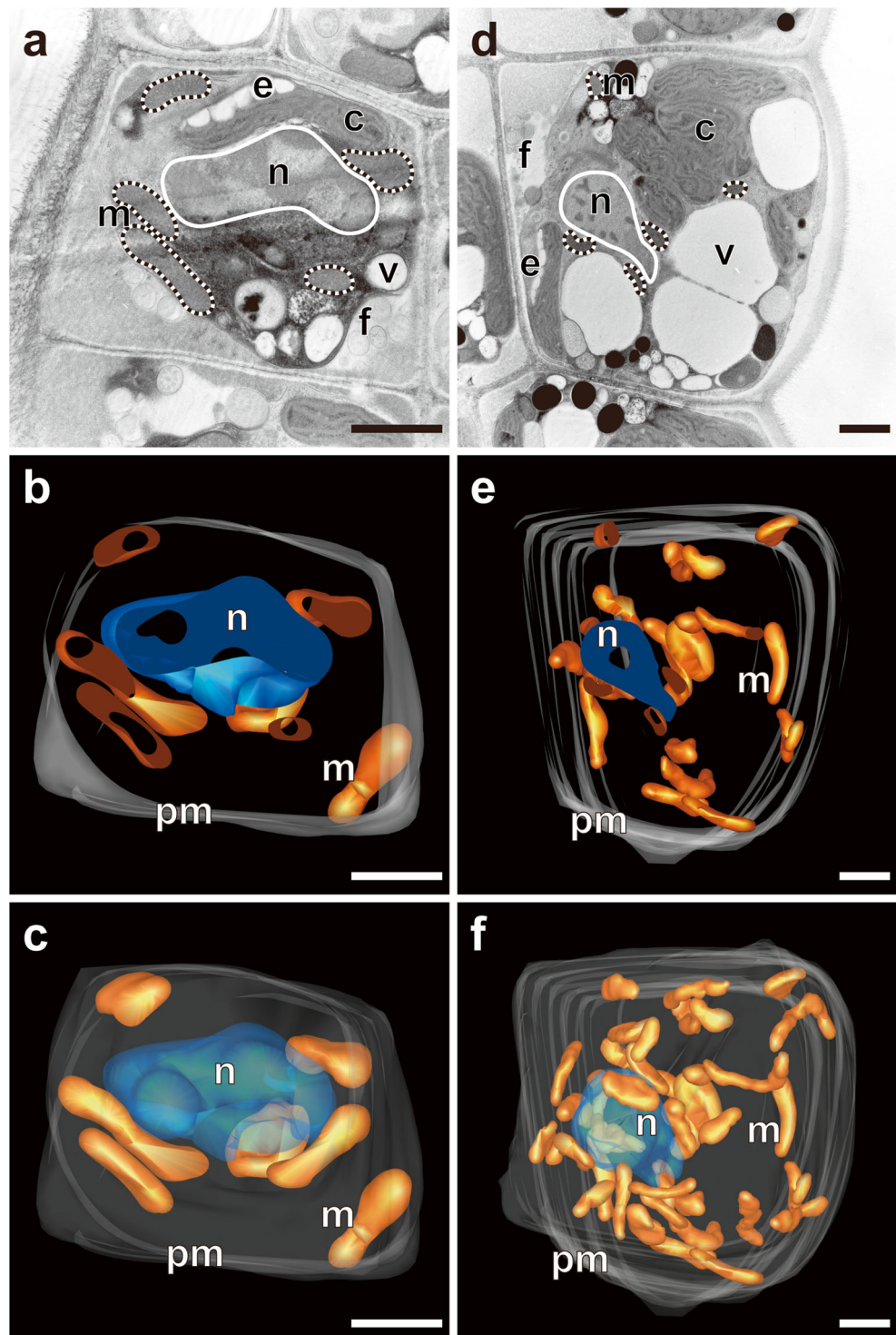
*M. cylindricus* possesses a heteromorphic life cycle alternating between the macroscopic haploid gametophytic generation and microscopic diploid sporophytic generation (Kitayama et al. 1992; Kawai et al. 2012; Supplementary Fig. S3). Male and female plants were independent, namely dioecious (Supplementary Fig. S3a, b). Gametophytes are parenchymatous, and mature plants have sori with many plurilocular gametangia (Supplementary Fig. S3c, d). Male gametophytes possess long, pale gametangia that produce male gametes, and female gametophytes exhibit short, dark brown gametangia that produce female gametes (Supplementary Fig. S3c–f). The cultured gametophytes established from gametes or trichothallic hairs of the materials from the field sample showed uniseriate filaments, and gametangia were directly

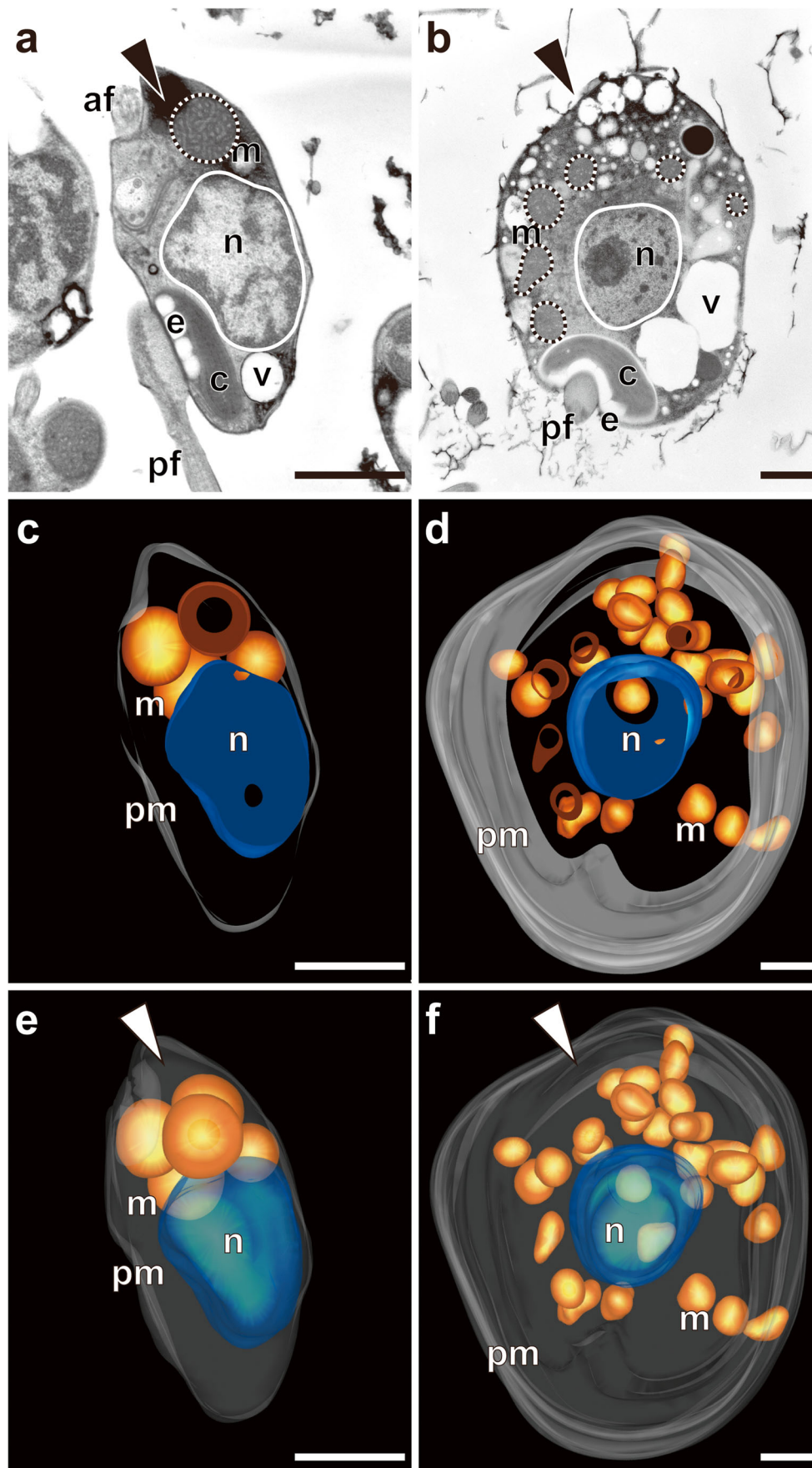
formed on the filaments. Observation of the mitochondrial structure in gametophyte cells was performed using the cultured materials. Supplementary Fig. S3g, h shows a 6-h-old zygote and a two-celled sporophyte, respectively. Two orange eyespots derived from male and female gametes remained. One 20-day-old crustose sporophyte is shown in Supplementary Figure S3i.

### Mitochondrial morphology in gametophytes

We first observed the ultrastructure of uniseriate filamentous male and female gametophytes (Fig. 1, Supplementary Movie S1, S2). The nucleus was generally located in the middle part of the cell (Fig. 1a, b), and chloroplasts and mitochondria were positioned in the perinuclear or pericytoplasmic regions by

**Fig. 2** Mitochondrial morphology in mature gametes from the plurilocular gametangia. **a–c** Male gamete in the gametangium, **d–f** female gamete in the gametangium. **a** A thin-section image of male gamete. **b** A partial 3D model of the nucleus, mitochondria, and plasma membrane reconstructed from serial thin sections in the same cell as **a**. **c** A complete 3D model of **b**. **d** A thin-section image of female gamete. **e** A partial 3D model of the nucleus, mitochondria, and plasma membrane reconstructed from serial thin sections in the same cell as **d**. **f** A complete 3D model of **e**. c, chloroplast; pm, plasma membrane; e, eyespot; f, flagellum; m, mitochondrion; n, nucleus; v, vacuole. Scale bar: 1  $\mu\text{m}$





◀ **Fig. 3** Mitochondrial morphology in gametes after release. **a, c, e** Male gamete, **b, d, f** female gamete. **a** A thin-section image of male gamete. **b** A thin-section image of female gamete. **c** A partial 3D model of the nucleus, mitochondria, and plasma membrane reconstructed from serial thin sections in the same cell as **a**. **d** A partial 3D model of the nucleus, mitochondria, and plasma membrane reconstructed from serial thin sections in the same cell as **b**. **e** A complete 3D model of **c**. **f** A complete 3D model of **d**. Arrowheads indicate the anterior part of the cell. c, chloroplast; pm, plasma membrane; e, eyespot; af, anterior flagellum; pf, posterior flagellum; m, mitochondrion; n, nucleus; v, vacuole. Scale bar: 1  $\mu\text{m}$

occupation of large vacuoles (Fig. 1a, b). Reconstruction of 3D images was performed by tracing the outline of the nucleus, mitochondria, and plasma membrane in the male and female gametophytes. Most mitochondria at this stage were tubular, curved, V-, or Y-shaped (Fig. 1c–f). The mitochondria were not branched and did not form interconnection networks.

We calculated the total number and total and mean volumes of mitochondria from three cells in each of the male and female gametophytes (Supplementary Table S1). There were 50, 83, and 117 mitochondria in the male gametophytes and 42, 59, and 104 in the female gametophytes. In the male gametophytes, the cells with the lowest number of mitochondria exhibited the highest total mitochondrial volume in the cell (“Male\_Gametophyte\_3” in Supplementary Table S1) because of variation in the mean volume of mitochondria in each male gametophyte (Supplementary Table S1). The mean values of the mitochondrial volume in the female gametophytes were not significantly different in each cell (Supplementary Table S1); therefore, the number of mitochondria reflected the total volume of the mitochondria in the cell. In this study, mitochondrial complexity was calculated to understand mitochondrial morphology (Vincent et al. 2019). The analysis showed that the mitochondria in each cell of the gametophytes exhibited considerable differences from spherical or elliptical geometries (Supplementary Table S1).

### Mitochondrial morphology in mature gametangia

Next, we examined mitochondrial morphology in mature male and female gametangia (Fig. 2, Supplementary Movie S3, S4). Mitochondrial morphology and distribution were determined through 3D analysis using three cells each of the male and female gametangia. In the mature male gametangia, two flagella were present and an eyespot was observed within the chloroplast adhered to the nucleus (Fig. 2a). Most mitochondria in the mature male gametangia showed a discoid shape (Fig. 2b, c). Similarly, the flagella and eyespots were also seen in the cells of mature female gametangia, and most mitochondria were tubular in shape with some discoid (Fig. 2d–f). In the cells of male and female gametangia, some mitochondria were located around the nucleus, while others were scattered in the cytoplasm. The number of mitochondria

examined in this study is summarized in Supplementary Table S1. Although the number of mitochondria is different in each cell, the variability in the numbers was not as large as in the gametophytes.

The average number of mitochondria in the cells of male and female gametangia was approximately 6 and 38, respectively. The difference in the total volume of the mitochondria in male or female gametangium was less compared to that observed in the gametophytic cells. In addition, the average mitochondrial volume in the male or female gametangia was approximately the same. The mitochondria in the cells of the male gametangia were slightly larger ( $0.162 \pm 0.013 \mu\text{m}^3$ ) than those in the cells of the female gametangia ( $0.133 \pm 0.004 \mu\text{m}^3$ ); however, there were no significant differences in the mitochondrial shape (Supplementary Table S2), as indicated by the MCI, between the male ( $1.682 \pm 0.091$ ) and female ( $1.852 \pm 0.074$ ) gametangia. The average MCI in the gametangia was lower than that in the gametophytes (male gametophytes,  $4.848 \pm 0.282$ ; female gametophytes,  $6.190 \pm 0.280$ ; Supplementary Table S1), indicating that the mitochondrial shape changed during gametogenesis.

### Mitochondrial morphology in male and female gametes

3D reconstruction of the male and female gametes released from the gametangia was performed next (Fig. 3, Supplementary Movie S5, S6). The shape of the mitochondria in the male and female gametes was nearly spherical (Fig. 3a, b). Most mitochondria were distributed in the anterior part of the gametes (Fig. 3c–f). The average mitochondrial number in three cells each of the male and female gametes was 5 and 27, respectively (Supplementary Table S1). A conspicuous decrease in the number of mitochondrial in female gametes prior to gamete release was confirmed. However, the total mitochondrial volume did not change before and after the release of gametes in both males and females. The average mitochondrial size was  $0.173 \pm 0.022 \mu\text{m}^3$  in male gametes and  $0.191 \pm 0.006 \mu\text{m}^3$  in female gametes, indicating that while female mitochondria were slightly larger than male mitochondria, the difference was not significant (Tukey’s multiple comparison  $P = 0.4593$ ; Supplementary Table S2). The MCI of the male and female mitochondria was  $0.758 \pm 0.007$  and  $1.034 \pm 0.042$ , respectively. According to these results, the shape of mitochondria in released gametes underwent a drastic change either during or after gamete release. Mitochondria in male gametes were nearly spherical (MCI  $\approx 0.71$ ) while the shape of mitochondria in female gametes was only slightly spherical (Supplementary Table S1). However, based on Tukey’s multiple comparison, the shapes of mitochondria in male and female gametes were significantly different from each other ( $P < 0.0001$ ; Supplementary Table S2).

## Mitochondrial morphology in early sporophytes

The disappearance of parental mitochondria in 2-h-old zygotes was observed (Shen et al. 2020). Mitochondrial morphology was examined in 2- and 6-h-old zygotes to compare the configuration of the maternal mitochondria during or after the disappearance of the paternal mitochondria (Fig. 4, Supplementary Movie S7, S8). Fertilization was confirmed by the number of eyespots on the chloroplasts derived from male and female gametes (Shen et al. 2020). Two eyespots were maintained until the formation of seven-celled sporophytes. The number of mitochondria in the three 2-h-old zygotes was 25, 26, and 35 (Supplementary Table S1). The zygote with 35 mitochondria (“2-h-old\_Zygote\_2” in Supplementary Table S1) appeared to have male mitochondria that had not yet been digested. In three 6-h-old zygotes, the number of mitochondria in each cell was 25, 29, and 30. The mean volume per mitochondrion in the 6-h-old zygotes was  $0.243 \pm 0.007 \mu\text{m}^3$ , which indicated that these had mitochondria increased in size compared to those in the 2-h-old zygotes ( $0.190 \pm 0.006 \mu\text{m}^3$ ), and this increase was statistically significant ( $P < 0.0001$ ; Supplementary Tables S1 and S2). However, the MCI values between the 2- and 6-h-old zygotes and the female gametes were not significantly different ( $P = 0.9997$ ; Supplementary Table S2).

The first cell division occurred symmetrically 24–48 h after fertilization. The morphology of mitochondria in 24-h-old zygotes was compared before and after cytokinesis (Fig. 5, Supplementary Movie S9, S10). The two zygotes examined before cytokinesis had either 32 or 33 mitochondria while the two zygotes examined after cytokinesis had either 31 or 34 mitochondria. Almost half of the mitochondria in each daughter cell were distributed from the mother cell (Supplementary Table S1). Dumbbell-shaped and elongated mitochondria were observed in the cells before cytokinesis (Fig. 5a–c). The number of mitochondria did not change toward the first cell division (Supplementary Table S1); however, the mitochondria became larger and adopted more complex shapes than those from 2- (Fig. 4a–c) and 6-h-old (Fig. 4d–f) zygotes. After cytokinesis, mitochondria in two-celled sporophytes were oval and tubular in shape, and the dumbbell-shaped mitochondria were no longer observed (Fig. 5d–f).

## Mitochondrial morphology in sporophytes

A cross-section of a 20-day-old crustose sporophyte is shown in Fig. 6 a. In the marginal meristematic cell layer, longer cells with asymmetric cytoplasmic distribution and shorter cells lacking large vacuoles were observed (Fig. 6b, c). We examined the mitochondria in a short cell (Fig. 6c–e, “20-d-old\_Sporophyte\_1” in Supplementary Table S1; Supplementary Movie S11). To compare the mitochondrial morphology among the cell layers, the cells positioned at the

subapical (Fig. 6f–h, “20-d-old\_Sporophyte\_2” in Supplementary Table S1; Supplementary Movie S12) and central regions (Fig. 6i–k, “20-d-old\_Sporophyte\_3” in Supplementary Table S1; Supplementary Movie S13) were examined. There were no significant differences in the total number and volume of mitochondria among the three cells examined (Supplementary Table S1). Tubular, curved, V-, and Y-shaped mitochondria were observed in all three cells (Fig. 6c–k). The MCI was highest in the subapical cell ( $4.180 \pm 0.250$ ), followed by the cell in the central region ( $3.363 \pm 0.203$ ). The marginal apical cell had the lowest MCI ( $2.463 \pm 0.147$ ) (Supplementary Table S1). There was little difference between the shapes of mitochondria in the central and subapical regions ( $P = 0.3047$ ; Supplementary Table S2); however, there was a statistically significant difference in the shape of the mitochondrial in the apical region from those in the subapical ( $P < 0.0001$ ) and central regions ( $P = 0.0264$ ; Supplementary Table S2).

The volume of each mitochondrion in non-gametophyte cells is summarized in Fig. 7. This analysis showed that the volume of mitochondria increased before and after cytokinesis; however, mitochondria in other stages were stable in volume.

## Discussion

### Ultrastructural studies through the generations of the life cycle in *M. cylindricus*

To understand the dynamics of mitochondrial morphology across generations in brown algae, we selected *M. cylindricus* because of the heteromorphic alternation of generations in its life cycles and its anisogamous sexual reproduction patterns. The mitochondria in the uniseriate filamentous gametophytes, mature gametangia, gametes, zygotes, and crustose sporophytes were examined through consecutive serial sections using TEM. Moreover, quantitative analysis based on the 3D images was performed to characterize the mitochondrial morphology at each stage of the life cycle. Observation of the ultrastructure throughout the life cycle of brown algae was previously performed in *Scytothamnus australis* and *Scytothamnus fasciculatus* (Clayton 1986) using cultured material. In that report, however, the mitochondrial structure was not described. The ultrastructure of mitochondria in the gametangia, sporangia, and gametes of brown algae has been reported (Brawley et al. 1976; La Claire and West 1978, 1979; Berkaloff and Rousseau 1979; Henry and Cole 1982a, b; Clayton 1984; Katsaros and Galatis 1986; Maier 1997); however, our study was the first to report mitochondrial morphological observations across generations and to quantify mitochondrial morphology in brown algae using 3D.

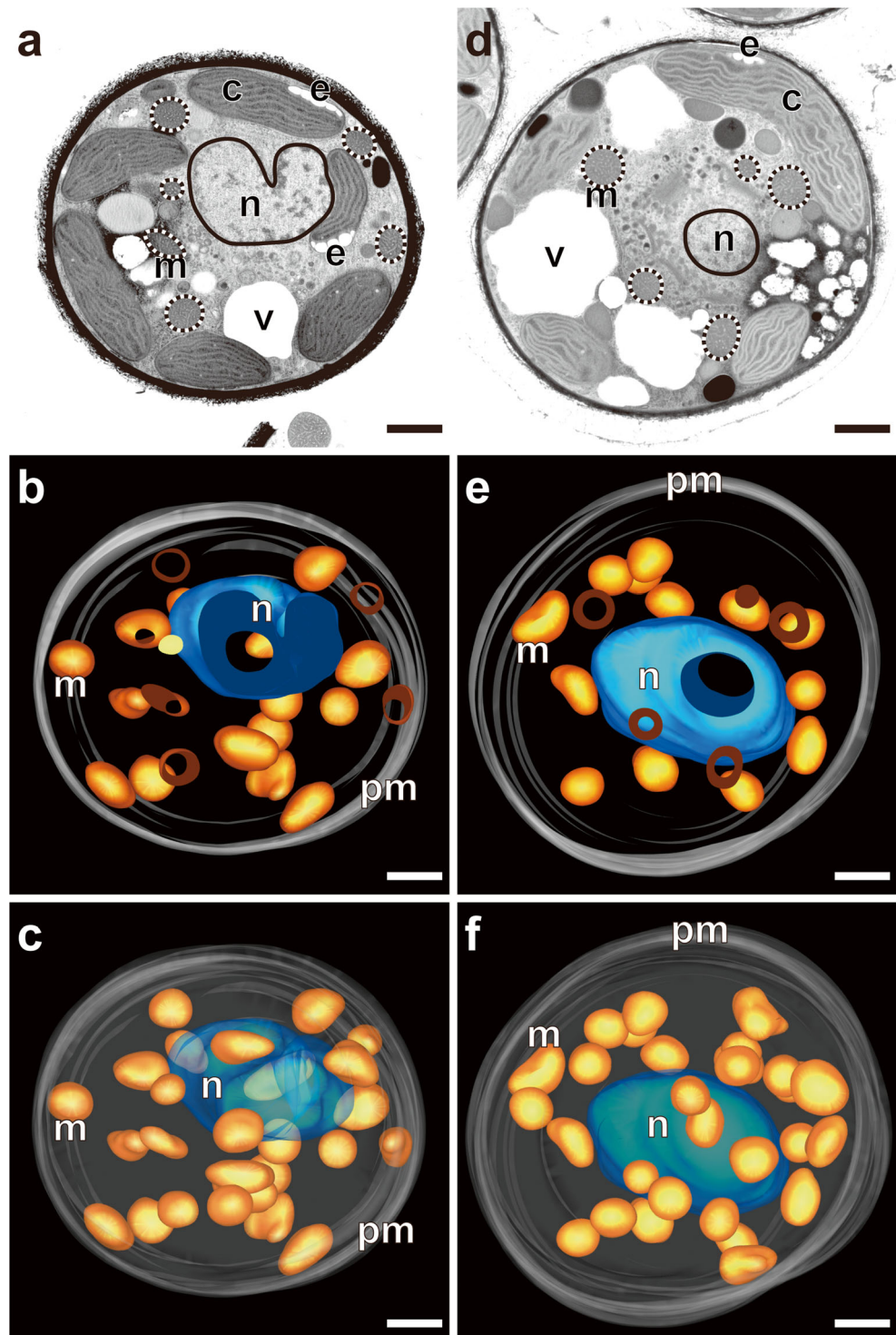


### Fusion of mitochondria at the final stage of female gametogenesis

In this study, 3D image reconstruction allowed us to quantitatively analyze the volume and complexity of the mitochondria. Mitochondria in gametes with two flagella and eyespots within the locules of the male and female gametangia in

*M. cylindricus* showed an elongated tubular shape; however, they were almost spherical in the released male and female gametes. The total number and volume of mitochondria contained in the released male gametes were similar to those in the cells before release (Figs. 2a–c and 3a, c, e, Supplementary Table S1). The mitochondrial morphology only changed immediately before release. In a similar analysis of

**Fig. 4** Mitochondrial morphology in 2- and 6-h-old zygotes. **a–c** A 2-h-old zygote, **d–f** a 6-h-old zygote. **a** A thin-section image of a 2-h-old zygote. **b** A partial 3D model of the nucleus, mitochondria, and plasma membrane reconstructed from serial thin sections in the same cell as **a**. **c** A complete 3D model of **b**. **d** A thin-section image of a 6-h-old zygote. **e** A partial 3D model of the nucleus, mitochondria, and plasma membrane reconstructed from serial thin sections in the same cell as **d**. **f** A complete 3D model of **e**. c, chloroplast; pm, plasma membrane; e, eyespot; m, mitochondrion; n, nucleus; v, vacuole. Scale bar: 1  $\mu\text{m}$

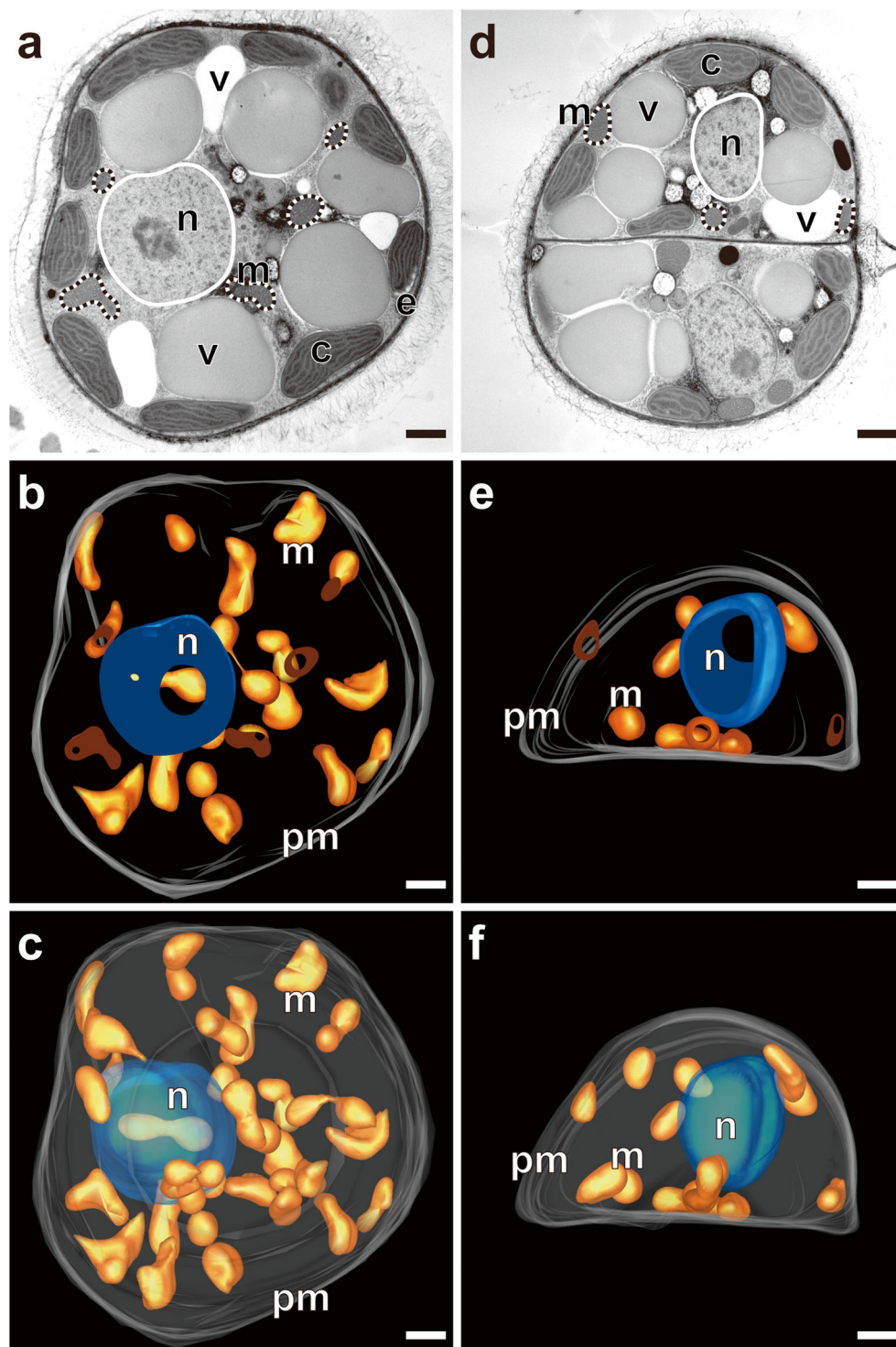


female gametes, the number of mitochondria diminished in the released gametes, and their total volume did not change from the gametes before release (Figs. 2d–f and 3b, d, f). These data suggest that mitochondrial fusion occurs in female gametes during the final stage of gametogenesis.

Fission and fusion of mitochondria constitute the mitochondrial dynamics, which are important processes for the

maintenance of mitochondrial quality (Varuzhanyan and Chan 2020). In particular, fusion promotes the elimination of mitochondrial diversity, such as mitochondrial DNA (mtDNA) and functional heterogeneity (Chan 2012). The fusion of mitochondria is observed at a specific stage of spermatogenesis in *Drosophila melanogaster* (Hales and Fuller 1997) in which the mitochondria aggregate and fuse to form

**Fig. 5** Mitochondrial morphology in 24-h-old zygotes. **a–c** A 24-h-old zygote before cytokinesis, **d–f** a 24-h-old zygote after cytokinesis. **a** A thin-section image of a 24-h-old zygote before cytokinesis. **b** A partial 3D model of the nucleus, mitochondria, and plasma membrane reconstructed from serial thin sections in the same cell as **a**. **c** A complete 3D model of **b**. **d** A thin-section image of the 24-h-old zygote after cytokinesis. **e** A partial 3D model of the nucleus, mitochondria, and plasma membrane reconstructed from serial thin sections in the same cell as **d**. **f** A complete 3D model of **e**. c, chloroplast; pm, plasma membrane; e, eyespot; m, mitochondrion; n, nucleus; v, vacuole. Scale bar: 1  $\mu$ m



the nebenkern, an onion-like giant mitochondrion. Mitochondria elongate during pachytene in meiosis I and fragment again after meiosis in rats (De Martino et al. 1979; Varuzhanyan et al. 2019). Mitochondrial fusion is considered particularly important for the production of healthy sperms. The mitochondrial fusion gene *fuzzy onions* (*Fzo*) was isolated from mutants showing male sterility in *D. melanogaster* (Hales and Fuller 1997). Mammalian homologs of FZO are mitofusins (Mfns) (Santel and Fuller 2001), and defects in the *MFN1* and *MFN2* genes induce the failure of sperm production (Varuzhanyan et al. 2019). Mitochondrial fusion-related genes were not found in the brown algae. However, based on a study on female gametogenesis in *M. cylindricus*, mitochondrial fusion occurs immediately before gamete release. In *M. cylindricus*, mtDNA is derived from female gametes, as reported previously (Shen et al. 2020). The mtDNA copy number in each mitochondrion in a male gamete is less than one-seventh of that in a female gamete. In addition, male mitochondria are digested by mitophagy after fertilization. It is possible that the fusion of mitochondria before the release of the female gametes could be a necessary final quality control step to unify the matrix and ensure the success of the maternal inheritance of mitochondria in this species.

## Mitochondrial complexity and cell types

Mitochondria in the vegetative gametophytes and sporophytes showed high MCI scores (Supplementary Table S1). Tubular, curved, V-, and Y-shaped mitochondria observed in these cells were not observed in other cells. The high MCI score for the mitochondria in these cells may be related to the development of large vacuoles within the cells (Figs. 1, 6). In a 20-day-old crustose sporophyte, mitochondrial morphology was analyzed using three cells collected from different regions of the alga. The results showed that the total and individual mitochondrial volumes were similar in all the cells. However, the MCI scores in the subapical and central regions were obviously higher (“20-d-old Sporophyte\_2” and “20-d-old Sporophyte\_3” in Supplementary Table S1) than those in the marginal apical region (“20-d-old Sporophyte\_1” in Supplementary Table S1). It was clear that the cytoplasm in the cell from the subapical region was occupied by a large vacuole compared to cells in the other regions (Fig. 7a). The complex morphology of mitochondria may thus be influenced to some extent by the development of vacuoles.

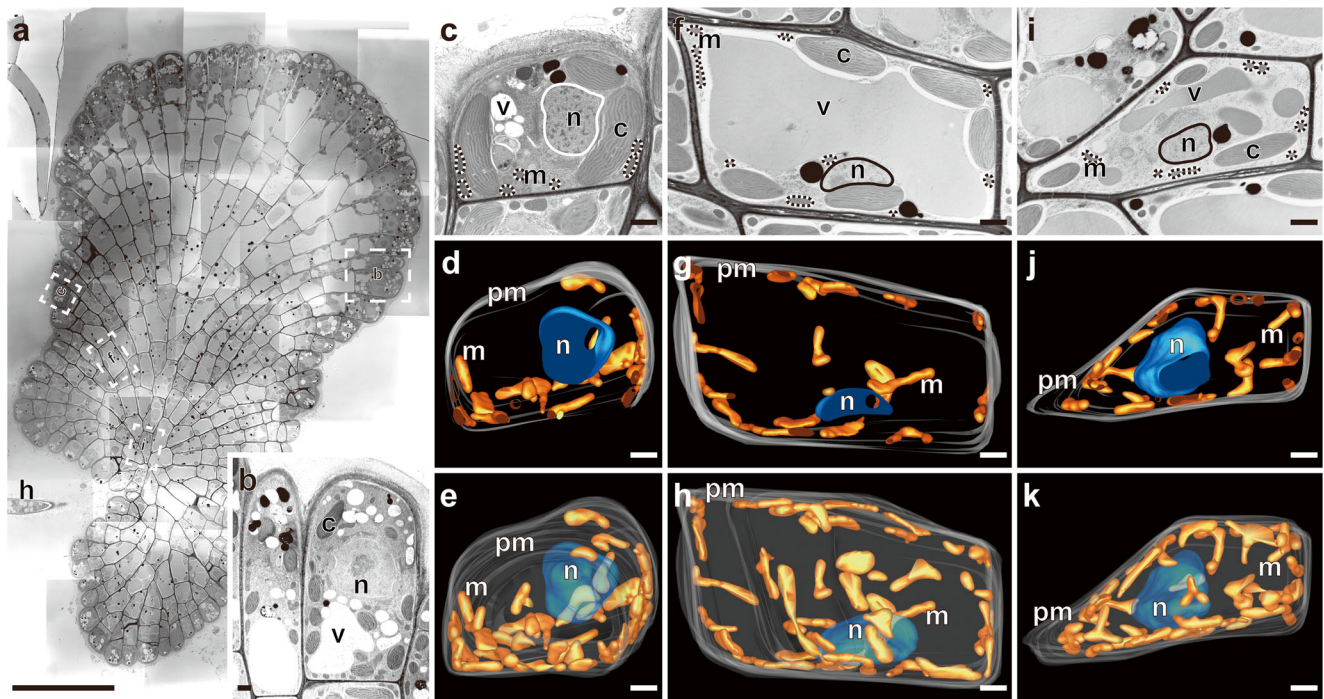


**Fig. 6** Mitochondrial morphology in a crustose sporophyte. **a** A thin-section image of a 20-day-old crustose sporophyte. **b** A thin-section image of a longer apical cell located in the marginal meristematic region in **a**. **c** A thin-section image of a shorter apical cell in the marginal meristematic region in **a**. **d** A partial 3D model of the nucleus, mitochondria, and plasma membrane reconstructed from serial thin sections in the same cell as **c**. **e** A complete 3D model of **d**. **f** A thin-section image of a cell in the subapical region in **a**. **g** A partial 3D model of the nucleus, mitochondria,

and plasma membrane reconstructed from the serial thin sections in the same cell as **f**. **h** A complete 3D model of **g**. **i** A thin-section image of a cell in the central region in **a**. **j** A partial 3D model of the nucleus, mitochondria, and plasma membrane reconstructed from serial thin sections in the same cell as **i**. **k** A complete 3D model of **j**. c, chloroplast; pm, plasma membrane; m, mitochondrion; n, nucleus; v, vacuole. Scale bar: 10  $\mu\text{m}$  in **a**; 1  $\mu\text{m}$  in **b–k**

## Mitochondrial structure in the vegetative and motile reproductive cells

Generally, mitochondria in brown algae are tubular. Moreover, in the most motile reproductive cells, the intercrystal structures—high electron-density structures—in the mitochondrial cristae are observed, for example, in the male and female gametes of *Cutleria hancockii* (La Claire and West 1978, 1979), *Scytosiphon lomentaria* (Clayton 1984), and *M. cylindricus* (Shen et al. 2020); the male gametes of *Ectocarpus siliculosus* (Maier 1997); zoospores of *Halopteris filicia* (Katsaros and Galatis 1986) and several species belonging to *Laminariales* (Henry and Cole 1982a); and sperm of *Fucus serratus* (Berkaloff and Rousseau 1979). The function of the intercrystal structure has not yet been elucidated, and the presence of this structure is limited in motile reproductive cells, not in eggs (Brawley et al. 1976). The occurrence of this structure was observed in mature, but not immature, gametangia in *Pylaiella littoralis* (Markey and Wilce 1975). The timing of the appearance of the tubular structure within the mitochondrial cristae may indicate the preparation of a switch from the vegetative to the reproductive type in the mitochondria. In this study, we did not examine the internal structure of the mitochondria. The mitochondria in both male and female gametes changed from a dumbbell or elongated shape to an almost spherical shape immediately before release. Morphological changes at the final stage of gametogenesis may be linked to the completion of optimal mitochondrial physiology in the motility cells. The timing of the disappearance of the intercrystal structure after fertilization or settlement of zoospores is unknown. In *M. cylindricus*, the mitochondrial size and MCI score increased 6 h after fertilization. It is thought that the physiological condition or function of the mitochondria may change from reproductive to vegetative type during this transition.

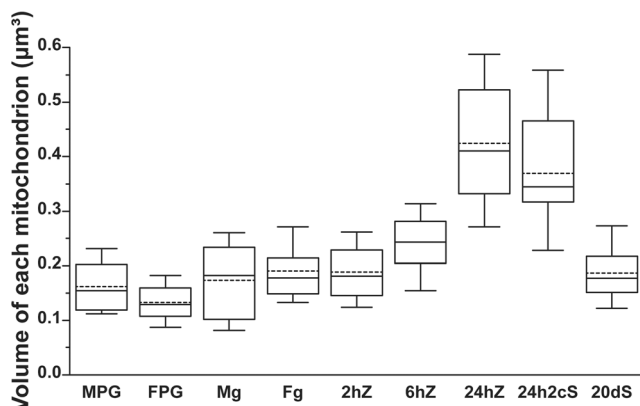


**Fig. 7** Box plot presenting quantitative analysis of each mitochondrial volume examined in the mature gametangia, released gametes, 1-day-old zygotes, and 2-day-old zygotes before and after cytokinesis. All mitochondria used for quantitative analysis originated from

## Conclusion

To understand the morphological dynamics in mitochondria across generations, we performed a quantitative analysis on mitochondria from *M. cylindricus* based on 3D reconstruction of serial sections imaged by TEM. It became clear that mitochondria in gametophytes and sporophytes showed high MCI scores compared to those in the gametes and during early development of the sporophytes, and this appeared to be related to the development of vacuoles in the cells. In the final stages of gametogenesis, a conspicuous reduction in the number of mitochondria in female gametes was observed. By comparing the total volume and the number of mitochondria in pre- and post-release female gametes, there is a strong possibility that mitochondria in the female gametes fuse immediately before release. This phenomenon suggests that mitochondria fuse to reduce heterogeneity and enhance maternal inheritance of mitochondria upon fertilization in this species. To verify this hypothesis, the continuous sequence of dynamic morphological changes in mitochondria needs to be further investigated.

**Supplementary Information** The online version contains supplementary material available at <https://doi.org/10.1007/s00709-021-01679-1>.

**Acknowledgements** We are grateful to Dr. Toyoki Iwao (Toba Fisheries Science Center) for collecting the fresh Mie-strain of *M. cylindricus*, and to Dr. Toshiaki Ito (Electron Microscope Laboratory, Research Faculty of Agriculture, Hokkaido University) for preparing the TEM samples of the gametophyte stage using high-pressure freezing.

**Author contribution** Yuan Shen analyzed the data and maintained the *M. cylindricus* strains. Chikako Nagasato and Taizo Motomura designed the experiments and critically reviewed the manuscript. All authors have written and edited the manuscript.

**Funding** This work was supported by the Sumitomo Foundation (grant number 190311).

## Declarations

**Conflict of interest** The authors declare no competing interests.

## References

- Aoyama H, Kuroiwa T, Nakamura S (2009) The dynamic behaviour of mitochondria in living zygotes during maturation and meiosis in *Chlamydomonas reinhardtii*. *Eur J Phycol* 44:497–507
- Berkaloff C, Rousseau B (1979) Ultrastructure of male gametogenesis in *Fucus serratus* (Phaeophyceae). *J Phycol* 15:163–173
- Brawley SH, Wetherbee R, Quatrano RS (1976) Fine-structural studies of the gametes and embryo of *Fucus vesiculosus* L. (Phaeophyta). II. The cytoplasm of the egg and young zygote. *J Cell Sci* 20:255–271
- Chan DC (2012) Fusion and fission: interlinked processes critical for mitochondrial health. *Annu Rev Genet* 46:265–287

- Clayton MN (1984) An electron microscope study of gamete release and settling in the complanate from *Scytosiphon* (Scytosiphonaceae, Phaeophyta). *J Phycol* 20:276–285
- Clayton MN (1986) Culture studies on the life history of *Scytothamnus australis* and *Scytothamnus fasciculatus* (Phaeophyta) with electron microscope observations on sporogenesis and gametogenesis. *Br Phycol J* 21:371–386
- Cui Y, Cao W, He Y, Zhao Q, Wakazaki M, Zhuang X, Gao J, Zeng Y, Gao C, Ding Y, Wong HY, Wong WS, Lam HK, Wang P, Ueda T, Rojas-Pierce M, Toyooka K, Kang BH, Jiang L (2019) A whole-cell electron tomography model of vacuole biogenesis in *Arabidopsis* root cells. *Nat Plants* 5:95–105
- De Martino C, Floridi A, Marcante ML, Malomi W, Scorza Barcellona P, Bellocci M, Silvestrini B (1979) Morphological, histochemical and biochemical studies on germ cell mitochondria of normal rats. *Cell Tissue Res* 196:1–22
- Ehara T, Osafune T, Hase E (1995) Behavior of mitochondria in synchronized cells of *Chlamydomonas reinhardtii* (Chlorophyta). *J Cell Sci* 108:499–507
- Fu G, Nagasato C, Ito T, Müller DG, Motomura T (2013) Ultrastructural analysis of flagellar development in plurilocular sporangia of *Ectocarpus siliculosus* (Phaeophyceae). *Protoplasma* 250:261–272
- Hales KG, Fuller MT (1997) Developmentally regulated mitochondrial fusion mediated by a conserved, novel, predicted GTPase. *Cell* 90:121–129
- Henry EC, Cole KM (1982a) Ultrastructure of swarmer in the Laminariales (Phaeophyceae). I. Zoospores. *J Phycol* 18:550–569
- Henry EC, Cole KM (1982b) Ultrastructure of swarmer in the Laminariales (Phaeophyceae). II. Sperm. *J Phycol* 18:570–579
- Ho HC, Wey S (2007) Three dimensional rendering of the mitochondrial sheath morphogenesis during mouse spermiogenesis. *Microsc Res Tech* 70:719–723
- Katsaros C, Galatis B (1986) Ultrastructural studies on zoosporogenesis of *Halopteris filicina* (Sphaelariales, Phaeophyta). *Phycologia* 25:358–370
- Kawai H, Kogishi K, Hanyuda T, Kitayama T (2012) Taxonomic revision of the genus *Cutleria* proposing a new genus *Mutimo* to accommodate *M. cylindricus* (Cutleriaceae, Phaeophyceae). *Psychol Res* 60:241–248
- Kinoshita N, Fu G, Ito T, Motomura T (2016) Three-dimensional organization of flagellar basal apparatus in *Ectocarpus* gametes. *Phycol Res* 64:19–25
- Kitayama T, Kawai H, Yoshida T (1992) Dominance of female gametophytes in field populations of *Cutleria cylindrica* (Cutleriaceae, Phaeophyceae) in the Tsugaru Strait, Japan. *Phycologia* 31:449–461
- Kremer JR, Mastroratte DN, McIntosh JR (1996) Computer visualization of three-dimensional image data using IMOD. *J Struct Biol* 116:71–76
- Kuroiwa T (2010) Mechanisms of organelle division and inheritance and their implications regarding the origin of eukaryotic cells. *Proc Jpn Acad Ser B Phys Biol Sci* 86:455–471
- La Claire JW, West JA (1978) Light and electron-microscopic studies of growth and reproduction in *Cutleria* (Phaeophyta). *Protoplasma* 97:93–110
- La Claire JW, West JA (1979) Light and electron-microscopic studies of growth and reproduction in *Cutleria* (phaeophyta). *Protoplasma* 101:247–267
- Lowe DG (2004) Distinctive image features from scale-invariant keypoints. *Int J Comput Vis* 60:91–110
- Maier I (1997) The fine structure of the male gamete of *Ectocarpus siliculosus* (Ectocarpales, Phaeophyceae). I. General structure of the cell. *Eur J Phycol* 32:241–253
- Markey DR, Wilce RT (1975) The ultrastructure of reproduction in the brown alga *Pylaiella littoralis*. I. Mitosis and cytokinesis in the plurilocular gametangia. *Protoplasma* 85:219–241
- Murtin C, Frindel C, Rousseau D, Ito K (2018) Image processing for precise three-dimensional registration and stitching of thick high-resolution laser-scanning microscopy image stacks. *Comput Biol Med* 92:22–41
- Nagasato C, Kajimura N, Terauchi M, Mineyuki Y, Motomura T (2014) Electron tomographic analysis of cytokinesis in the brown alga *Silvetia babingtonii* (Fucales, Phaeophyceae). *Protoplasma* 251:1347–1357
- Nagasato C, Motomura T (2002) Ultrastructural study on mitosis and cytokinesis in *Scytosiphon lomentaria* zygotes (Scytosiphonales, Phaeophyceae) by freeze-substitution. *Protoplasma* 219(3–4):140–149
- Nicander L, Ploen L (1969) Fine structure of spermatogonia and primary spermatocytes in rabbits. *Z Zellforsch Mikrosk Anat* 99:221–234
- Peachey LD (1958) Thin sections: I. A study of section thickness and physical distortion produced during microtomy. *J Biophys Biochem Cytol* 4:233–242
- Provasoli L (1968) Media and prospects for the cultivation of marine algae. In: Watanabe A, Hattori A (eds) Culture and collections of algae (Proc Jap Conf Hakone, 1966). Japanese Society of Plant Physiology, Tokyo, pp 63–75
- Rantanen A, Larsson NG (2000) Regulation of mitochondrial DNA copy number during spermatogenesis. *Hum Reprod* 2:86–91
- Santel A, Fuller MT (2001) Control of mitochondrial morphology by a human mitofusin. *J Cell Sci* 114:867–874
- Sato M, Sato K (2013) Maternal inheritance of mitochondrial DNA by diverse mechanisms to eliminate paternal mitochondrial DNA. *Biochim Biophys Acta* 1833:1979–1984
- Schindelin L, Arganda-Carreras I, Frise E, Kaynig V, Longair M, Pietzsch T, Preibisch S, Rueden C, Saalfeld S, Schmid B, Tinevez JY, White DJ, Hartenstein V, Eliceiri K, Tomancak P, Cardona A (2012) Fiji: an open-source platform for biological-image analysis. *Nat Methods* 28:676–682
- Shen Y, Iwao T, Motomura T, Nagasato C (2020) Cytoplasmic inheritance of mitochondria and chloroplasts in the anisogamous brown alga *Mutimo cylindricus*. *Protoplasma*:1–14
- Terauchi M, Nagasato C, Kajimura N, Mineyuki Y, Okuda K, Katsaros C, Motomura T (2012) Ultrastructural study of plasmodesmata in the brown alga *Dictyota dichotoma* (Dictyotales, Phaeophyceae). *Planta* 236:1013–1126
- Varuzhanyan G, Chan DC (2020) Mitochondrial dynamics during spermatogenesis. *J Cell Sci* 133:14
- Varuzhanyan G, Rojansky R, Sweredoski MJ, Graham RL, Hess S, Ladinsky MS, Chan DC (2019) Mitochondrial fusion is required for spermatogonial differentiation and meiosis. *elife* 8:e51601
- Vincent AE, White K, Davey T, Philips J, Ogden RT, Lawless C, Warren C, Hall MG, Ng YS, Falkous G, Holden T, Deehan D, Taylor RW, Turnbull DM, Picard M (2019) Quantitative 3D mapping of the human skeletal muscle mitochondrial network. *Cell Rep* 26:996–1009
- Yoshida Y, Kuroiwa H, Shimada T, Masaki Yoshida M, Mio Ohnuma M, Takayuki Fujiwara T, Yuuta Imoto Y, Fumi Yagisawa F, Keiji Nishida K, Shunsuke Hirooka S, Osami Misumi O, Yuko Mogi Y, Yoshihiko Akakabe Y, Kazunobu Matsushita K, Tsuneyoshi Kuroiwa T (2017) Glycosyltransferase MDR1 assembles a dividing ring for mitochondrial proliferation comprising polyglucan nanofilaments. *Proc Natl Acad Sci U S A* 114:13284–13289